Effect of Tilt Angle on Subcritical/Supercritical Carbon Dioxide-Based Natural Circulation Loop With Isothermal Source and Sink

Ajay Kumar Yadav[1]
Assistant Professor
Department of Mechanical Engineering,
National Institute of Technology Karnataka,
Surathkal, Mangalore 575 025, Karnataka, India
e-mail: ajayyadav.aba@rediffmail.com

M. Ram Gopal
Professor
Department of Mechanical Engineering,
Indian Institute of Technology Kharagpur,
Kharagpur 721 302, India
e-mail: ramg@mech.iitkgp.ernet.in

Souvik Bhattacharyya
Professor
Department of Mechanical Engineering,
Indian Institute of Technology Kharagpur,
Kharagpur 721 302, India
e-mail: souvik.iit@gmail.com

In recent years, a growing popularity of carbon dioxide (CO_2) as a secondary fluid has been witnessed in both forced as well as in natural circulation loops (NCLs). This may be attributed to the favorable thermophysical properties of CO_2 in addition to the environmental benignity of the fluid. However, an extensive literature review shows that studies on CO_2-based NCLs are very limited. Also, most of the studies on NCLs do not consider the three-dimensional variation of the field variables. In the present work, three-dimensional computational fluid dynamics (CFD) models of a NCL with isothermal source and sink have been developed to study the effect of tilt angle in different planes. Studies have been carried out employing subcritical (liquid and vapor) as well as supercritical phase of CO_2 as loop fluid at different operating pressures and temperatures. Results are obtained for a range of tilt angles of the loop, and a significant effect is observed on heat transfer, mass flow rate, and stability of the loop. It was also found that changing the orientation of the loop could be an elegant and effective solution to the flow instability problem of NCLs. [DOI: 10.1115/1.4030702]

Keywords: natural circulation loop, CFD, heat transfer, turbulent flow, carbon dioxide

1 Introduction

NCL is safe and reliable due to absence of any moving components such as pumps and compressor. It removes heat from a source and transports it to a sink located at higher elevation by means of buoyancy caused by temperature difference between source and sink. NCLs are widely used in applications such as refrigeration and air-conditioning systems, solar collectors, and nuclear reactors. In recent years, CO_2 has been found to be suitable as a secondary fluid in both forced convection loops as well as in NCLs [1–3] and has been proposed for various applications such as new generation nuclear reactors [4], chemical extraction [5,6], cryogenic refrigeration [7], heat pump [8], electronic cooling systems [9], and geothermal applications [10,11]. This may be attributed to the favorable thermophysical properties of CO_2 (shown in Table 1) in addition to its environment friendliness [12,13]. Studies show that for low temperature refrigeration and air-conditioning applications, CO_2-based NCLs are more compact in comparison to other conventional working fluids [2] and have been proposed for various heat transfer applications such as geothermal [10,11,14], solar collector [15], Stirling cooler [16], and heat pump [8,17]. However, an NCL may be subjected to the problem of instability, due to which the magnitude and direction of fluid flow may fluctuate in time. Many researchers [18–23] have reported and studied the problem of instability in NCLs. Instability problem becomes prominent if the loop is geometrically as well as thermally symmetrical. Studies show that tilting the loop may offer a solution to the stability problems [24,25]. However, effect of tilt angles on heat transfer and stability of CO_2-based NCL with isothermal source and sink is not available in open literature. In the present study, a CO_2 loop is considered and effect of tilt angles on heat transfer and stability of the loop are studied. Results are presented on the transient behavior of the loop at various operating pressures and temperatures. The operating parameter range is chosen such that the loop fluid (CO_2) exists either in a subcritical state or in a supercritical state.

2 Physical Model and Mathematical Formulations

2.1 Physical Model. Figure 1(*a*) shows the schematic of a 3D rectangular NCL which consists of an isothermal sink, an isothermal source, and left and right insulated legs. The loop fluid is heated sensibly in the isothermal source (T_H) and is cooled sensibly in the isothermal sink (T_C). Circulation of the loop fluid is maintained due to the buoyancy effect caused by heating at the bottom and cooling at the top.

Studies are carried out at different tilt angles of the loop in *XY* and *YZ* planes. Figure 1(*b*) shows the rotation of the loop in *XY* plane in clockwise direction. The loop is considered to be vertical at a tilt angle of 0 deg. The loop is also tilted in the *YZ* plane from vertical position in counterclockwise direction as depicted in

Table 1 Comparison of thermophysical properties of CO_2 ($P = 60$ bar (liquid) and $P = 90$ bar (supercritical)) with water ($P = 1$ atm) at same temperature [12]

Ratio	β	c_p	λ	μ	ρ
Liquid CO_2/water ($T = 283$ K)	101	0.64	0.18	0.07	0.88
Supercritical CO_2/water ($T = 313$ K)	256	3.06	0.11	0.05	0.5

[1]Corresponding author.

Contributed by the Heat Transfer Division of ASME for publication in the Journal of Thermal Science and Engineering Applications. Manuscript received April 26, 2014; final manuscript received October 24, 2014; published online November 11, 2015. Assoc. Editor: Bengt Sunden.

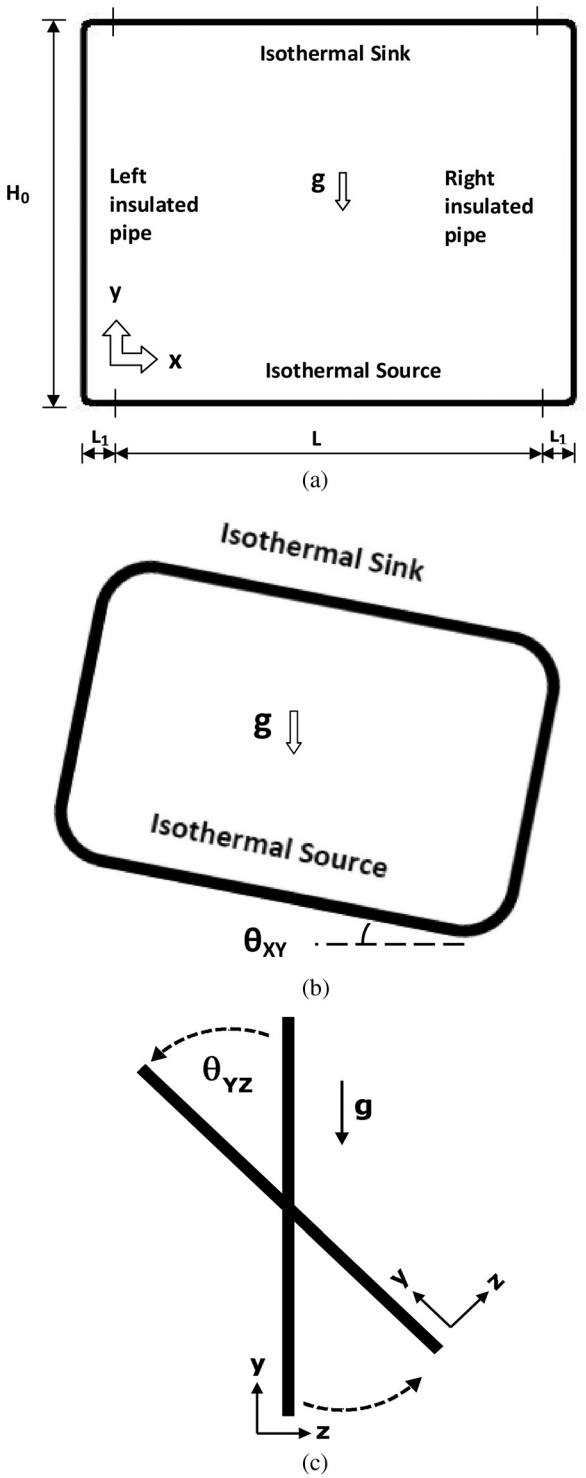

Fig. 1 (*a*) Schematic of the NCL employed in the model, (*b*) rotation of the loop in *XY* plane (front view), and (*c*) rotation of the loop in *YZ* plane (side view)

Fig. 1(*c*). Geometric and material specifications of the model are given in Table 2. In the present studies, the fluid flow is turbulent in all cases.

The following simplifying assumptions are made in the analysis:

(a) The loop fluid is in single-phase throughout the loop.
(b) The left and right vertical legs of the loop are perfectly insulated (adiabatic).

Table 2 Geometric and material specifications for the model

Parameter	Value
Internal diameter of the loop (d)	15 mm
Length of isothermal sink or source (L)	120 cm
Total width of the loop (L_0)	146 cm
Total height of the loop (H_0)	124.5 cm
Total length of the loop (L_t)	545 cm
Insulated pipe length in horizontal pipe ($2L_1$)	26 cm
Radius of curvature for bend (R)	30 mm
Tube wall thickness	2 mm
Material of the loop	Copper

(c) Wall material is isotropic with constant thermal conductivity.

2.2 Mathematical Formulation and Solution. The standard conservation equations with unsteady terms are shown below. These equations with relevant boundary conditions are solved by the commercial software, ANSYS (FLUENT) 14.5.

Conservation of mass

$$\frac{\partial \rho}{\partial t} + \nabla \cdot (\rho \mathbf{V}) = 0 \tag{1}$$

Conservation of momentum (Navier–Stokes equation) is expresses as

$$\frac{\partial (\rho \mathbf{V})}{\partial t} + \nabla \cdot (\rho \mathbf{V}\mathbf{V}) = -\nabla p + \nabla \cdot (\bar{\bar{\tau}}) + \rho \mathbf{g} \tag{2}$$

where the stress tensor can be written as

$$\bar{\bar{\tau}} = \mu \left[(\nabla \mathbf{V} + \nabla \mathbf{V}^{\mathrm{T}}) - \frac{2}{3} \nabla \cdot \mathbf{V} I \right]$$

Second term in stress tensor is the effect of volume dilation, and I is the unit tensor.

Conservation of energy with viscous dissipation may be expressed as

$$\frac{\partial (\rho E)}{\partial t} + \nabla \cdot (\mathbf{V}(\rho E + p)) = \nabla \cdot \left(\lambda_{\mathrm{eff}} \nabla T + \bar{\bar{\tau}} \cdot \mathbf{V} \right) \tag{3}$$

where

$$E = \int_{T_{\mathrm{ref}}}^{T} C_{\mathrm{p}} dT + \frac{V^2}{2} \tag{4}$$

and $T_{\mathrm{ref}} = 298.15$ K.

2.2.1 Model for Turbulence Analysis. Turbulent models for supercritical fluid are less developed and still under intense study [26]. Therefore, in the present simulation, a general *renormalization group* (RNG) k–ε model is employed to introduce the expression of turbulent effect. This method has also been used successfully in previous studies on supercritical CO_2 turbulent flow yielding accurate results [27,28].

The transport equations for RNG k–ε model are written as

$$\frac{\partial}{\partial t}(\rho k) + \frac{\partial}{\partial x_i}(\rho k u_i) = \frac{\partial}{\partial x_j}\left(\alpha_k \mu_{\mathrm{eff}} \frac{\partial k}{\partial x_j} \right) + G_{\mathrm{k}} + G_{\mathrm{b}} - \rho \varepsilon \tag{5}$$

$$\frac{\partial}{\partial t}(\rho \varepsilon) + \frac{\partial}{\partial x_i}(\rho \varepsilon u_i) = \frac{\partial}{\partial x_j}\left(\alpha_\varepsilon \mu_{\mathrm{eff}} \frac{\partial \varepsilon}{\partial x_j} \right) + C_{1\varepsilon} \frac{\varepsilon}{k}(G_{\mathrm{k}} + C_{3\varepsilon} G_{\mathrm{b}}) - C_{2\varepsilon} \rho \frac{\varepsilon^2}{k} - R_\varepsilon \tag{6}$$

where G_k and G_b are the generation of turbulence kinetic energy due to the mean velocity gradients and buoyancy, respectively,

$$G_k = \mu_t S^2 \tag{7}$$

where S is the modulus of the mean rate-of-strain tensor, defined as

$$S \equiv \sqrt{2S_{ij}S_{ij}} \tag{8}$$

S_{ij} is the rate-of-strain tensor defined as

$$S_{ij} \equiv \frac{1}{2}\left(\frac{\partial u_i}{\partial x_i} + \frac{\partial u_j}{\partial x_i}\right) \tag{9}$$

$$\mu_t = \rho C_\mu k^2/\varepsilon \tag{10}$$

Generation of turbulence due to buoyancy is given by

$$G_b = \beta g_i \frac{\mu_t}{\mathrm{Pr}_t}\frac{\partial T}{\partial x_i} \tag{11}$$

where

$$\beta = -\frac{1}{\rho}\left(\frac{\partial \rho}{\partial T}\right)_p \tag{12}$$

$$\mathrm{Pr}_t = 1/\alpha \tag{13}$$

$$\left|\frac{\alpha - 1.3929}{\alpha_0 - 1.3929}\right|^{0.6321}\left|\frac{\alpha + 2.3929}{\alpha_0 + 2.3929}\right|^{0.3679} = \frac{\mu}{\mu_{\mathrm{eff}}} \tag{14}$$

$$\alpha_0 = 1/\mathrm{Pr} = \lambda/\mu c_p \tag{15}$$

$$R_\varepsilon = \frac{C_\mu \rho \eta^3 (1 - \eta/\eta_0)\varepsilon^2}{(1 + 0.012\eta^3)k} \tag{16}$$

where $\eta \equiv Sk/\varepsilon$; $\eta_0 = 4.38$; $C_\mu = 0.0845$; $\alpha_k = \alpha_\varepsilon = 1.393$; $C_{1\varepsilon} = 1.42$; and $C_{2\varepsilon} = 1.68$

$$C_{3\varepsilon} = \tanh\left|\frac{v}{u}\right| \tag{17}$$

v is the component of the flow velocity parallel to the gravitational vector, and u is the component of the flow velocity perpendicular to the gravitational vector.

Equation for the effective viscosity is given by

$$d\left(\frac{\rho^2 k}{\sqrt{\varepsilon\mu}}\right) = 1.72\frac{\hat{v}}{\sqrt{\hat{v}^3 - 1 + C_v}}d\hat{v} \tag{18}$$

where

$$\hat{v} = \mu_{\mathrm{eff}}/\mu \tag{19}$$

and $C_v \approx 100$.

Effective conductivity is expressed as

$$\lambda_{\mathrm{eff}} = \alpha C_p \mu_{\mathrm{eff}} \tag{20}$$

The following terms are defined to describe the fluid flow and heat transfer phenomena.

Mass flow rate at any cross section is defined as

$$m = \int_0^A \rho V dA \tag{21}$$

Local bulk mean temperature of the fluid is expressed as

$$T = \frac{\int_0^A c_p T \rho V dA}{\int_0^A c_p \rho V dA} \tag{22}$$

Steady-state Reynolds number and modified Grashof number [29] are defined as

$$\mathrm{Re} = \frac{4m}{\pi d\mu} \tag{23}$$

$$\mathrm{Gr}_m = \frac{g\beta d^3 \rho^2 Q H_0}{A\mu^3 c_p} \tag{24}$$

where Q is the heat transfer rate from heat source to the sink.

Heat transfer rate at source/sink wall

$$Q = -\int_0^A \left(\lambda\frac{\partial T}{\partial r}\right)dA = \int_0^A h(T_s - T_f)dA \tag{25}$$

where $\bar{h}$ is the area-weighted average wall function heat transfer coefficient for isothermal source or sink

$$\bar{h} = \frac{\int_0^A h dA}{\int_0^A dA} \tag{26}$$

All the properties are calculated at the bulk mean temperature (T_m) of the loop fluid, defined as

$$T_m = \frac{\sum_{i=1}^{n} T_i}{n} \tag{27}$$

where n is the number of cross sections considered in the loop.

Average temperature of the loop is defined as

$$T_{\mathrm{avg}} = \frac{T_C + T_H}{2} \tag{28}$$

where T_C and T_H are isothermal wall temperatures of sink and source, respectively.

For wall conduction

$$\nabla^2 T = \frac{1}{\alpha}\frac{\partial T}{\partial t} \tag{29}$$

Boundary conditions

(i) No-slip and no-penetration boundary conditions are applied near the walls.
(ii) All external walls except source and sink are perfectly insulated.
(iii) For internal walls, conjugate heat transfer is considered.
(iv) Source and sink temperatures are known boundary conditions.

2.2.2 Simulation Details. The governing equations for mass, momentum, and energy are solved employing the CFD code, ANSYS 14.5 (FLUENT). A 3D geometry was prepared and transient simulation was carried out, where the implicit-coupled finite-volume method was used to discretize the governing equations. The *pressure-implicit with splitting of operators* algorithm was used to solve the coupling model between velocity and pressure.

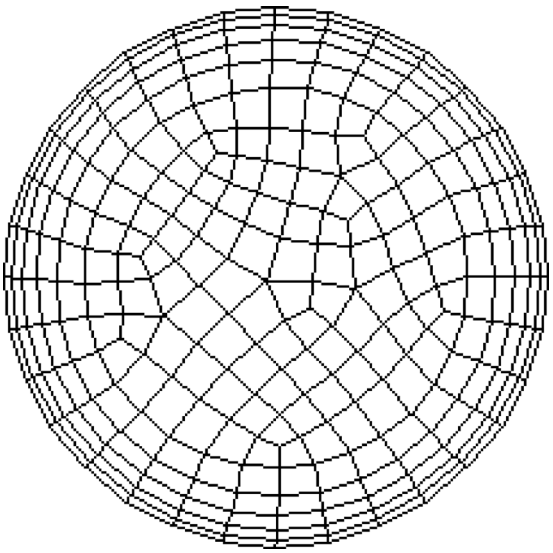

Fig. 2 Meshing of a cross section (fluid part only)

This method has also been used successfully in previously reported relevant studies [23,28,30,31].

The momentum and energy terms in the governing equations are iterated with a second-order upwind scheme that uses the upstream values and gradients to compute the control volume face values. Turbulence parameters (k, ε, etc.) are also iterated with a second-order upwind scheme. The *pressure staggering option* scheme is used to discretize the pressure term. For the near wall treatment, a standard wall function has been assumed in case of turbulent flow [32]. Axial conduction and viscous dissipation in fluid are considered, while axial conduction along the tube wall is incorporated as well. Convergence is obtained when various residuals of the parameters (temperature, velocity, pressure, etc.) change with the iterations within a preset convergence criterion of 10^{-3} for the residuals of continuity equation and 10^{-6} for the energy equation. Conservation of mass and energy are also checked for all the cases in the analysis.

Figure 2 shows the meshing of a cross section of the loop which has a minimum grid size of 0.2 mm in radial direction near the wall and increases to the maximum grid size of 0.8 mm away from the wall. Coarse meshing is adopted in the axial direction (5 mm grid size in horizontal pipes including bends and 10 mm for vertical pipes). Mesh generation yielded a total of 235,552 nodes. The values of Y^+ and Y^* have been checked for all the cases of turbulent flow to ensure optimal choice of fineness of grid. Maximum Y^+ and Y^* values in the present study are 54.5 and 54.4, respectively, which ensure that the grid is suitable for the assumption of standard wall function near the wall [32]. Grid independence tests were carried out and results with fine and coarse grids were compared (Table 3). In case of fine grid, 0.1 mm grid size was considered near the wall and 0.4 mm away from the wall; in case of coarse grid, a 0.3 mm grid size was considered near the wall and 1.2 mm away from the wall. Results are obtained for a loop operating pressure of 90 bar with source and sink temperature of 323 K and 305 K, respectively. Performance of the loop is presented in terms of mass flow rate (m) and heat transfer rate (Q). It may be noted that the differences between coarse and fine grid results are within 1%.

Table 3 Grid independence test for operating pressure 90 bar, sink and source temperatures 305 K and 323 K, respectively

Minimum grid size (mm)	No. of nodes	Heat transfer rate (W)	Mass flow rate (kg/s)
0.1	387,000	2239	0.07932
0.2	235,552	2217	0.07803
0.3	140,085	2174	0.07569

Table 4 Operating pressure and temperature

State of loop fluid	Pressure (bar)	T_C (K)	T_H (K)
Subcritical liquid	70	274	292
Subcritical vapor	70	305	323
Supercritical	90	305	323

2.3 Calculation of Thermophysical Properties of CO_2. Since the studies are carried out for subcritical (liquid and vapor) as well as supercritical states of CO_2 close to critical points where the variation in thermophysical properties is extremely large, it is essential to adequately capture the property variation due to changes in temperature. However, as shown in the literature, due to very small variation in operating pressure throughout the NCL, the effect of variation of pressure on the properties of single-phase CO_2 is not expected to be significant [30,33]. Hence, for a given operating pressure, the properties of CO_2 at any point in the loop are calculated at the fixed operating pressure and local temperature. The required properties of CO_2 including density, specific heat, thermal conductivity, and viscosity are obtained from the NIST Standard Reference Database REFPROP Version 9.1 [12]. Properties of CO_2 for the operating temperature range at a temperature difference of 1 K are added to the fluid properties library, and a piecewise-linear interpolation approach is used to calculate the properties within 1 K temperature difference.

3 Results and Discussion

This study has been conducted for tilt angle varying from 0 to 45 deg in *XY* and *YZ* planes. Subcritical (liquid and vapor) and supercritical CO_2 are considered for the study. The operating temperature range is chosen in such a way that it covers the subcritical and supercritical region of CO_2 and would be useful for various engineering applications involving transport of heat. Operating pressure of the loop is defined at the center of the isothermal source. For transient studies, sink temperature is considered as initial temperature of the loop.

Operating pressures and temperatures considered in the study are shown in Table 4. Temperature difference between isothermal source and sink is kept constant at 18 K.

3.1 Variation of Temperature and Velocity Throughout the Loop. Figures 3(*a*)–3(*d*) show the variation of local average temperature and velocity of CO_2 throughout the loop for different tilt angles in *XY* and *YZ* planes for supercritical case. Since temperature of sink (305 K) and source (323 K) are kept constant, therefore no significant effect of tilt angles on temperature is observed (Figs. 3(*a*) and 3(*b*)). Variation of temperature throughout the loop can be seen in the results for both the cases due to temperature difference between source and sink. Effect of tilt angles on velocity can be observed from Figs. 3(*c*) and 3(*d*) for both the planes *XY* and *YZ*, respectively. Results show that at higher tilt angles, velocity is lower which occurs due to decrease in effective height of the loops as tilt angle increases.

3.2 Effect of Tilt on Heat flux. Figures 4(*a*) and 4(*b*) show the effect of tilt angles in *XY* and *YZ* planes on heat flux, respectively. Results are obtained for constant ΔT (temperature difference between isothermal source and sink) of 18 K at different source and sink temperatures. Results show that if angle of tilt

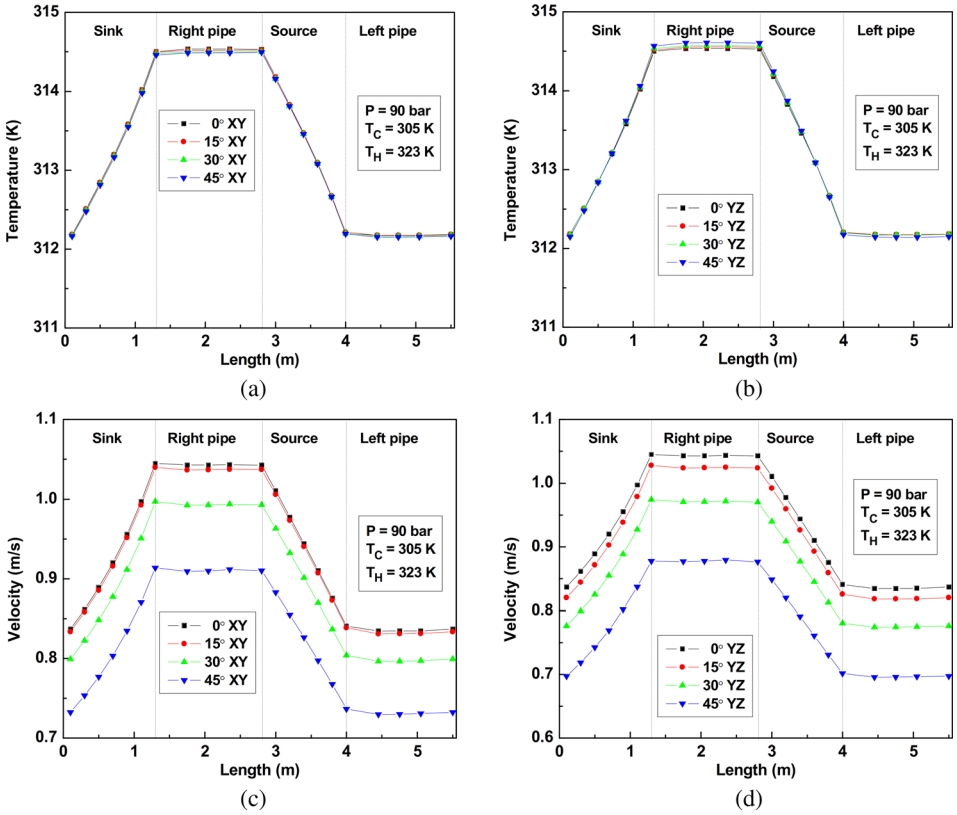

Fig. 3 (*a*) Variation of temperature throughout the loop for different tilt angles in *XY* plane, (*b*) variation of temperature throughout the loop for different tilt angles in *YZ* plane, (*c*) variation of velocity throughout the loop for different tilt angles in *XY* plane, and (*d*) variation of velocity throughout the loop for different tilt angles in *YZ* plane

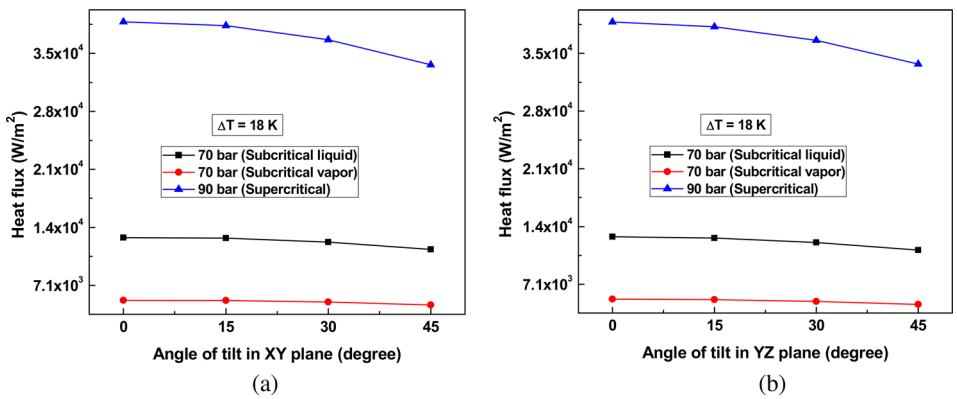

Fig. 4 (*a*) Variation in heat flux rate with angle of tilt in *XY* plane and (*b*) variation in heat flux rate with angle of tilt in *YZ* plane

increases heat flux decreases in both the planes which may be ascribed to decrease in effective height of the loop.

It can also be seen from the results that the heat flux in the case of supercritical phase is very high compared to subcritical phase. This occurs due to the operating of loop near pseudocritical region in supercritical phase [13,31]. Near pseudocritical region, the working fluid thermophysical properties are favorable for NCLs. Thermophysical properties near pseudocritical region in supercritical phase are given in Table 1. Very high volumetric expansion coefficient, very low viscosity, and higher specific heat capacity near pseudocritical point cause higher heat flux/heat transfer rate in the supercritical phase.

3.3 Effect of Tilt on Mass Flow Rate. Figures 5(*a*) and 5(*b*) show the effect of tilt angles in *XY* and *YZ* planes on mass flow rate, respectively. Results show that if angle of tilt increases, mass flow rate decreases in both the planes due to decrease in effective height of the loop. Decrease in mass flow rate decreases the Reynolds number and hence the heat transfer coefficient.

3.4 Effect of Isothermal Source Temperature on Heat Flux. Figure 6 shows the effect of isothermal source temperature on heat flux/heat transfer rate for different angles of tilt. Heat transfer rate depends on temperature difference (ΔT) and

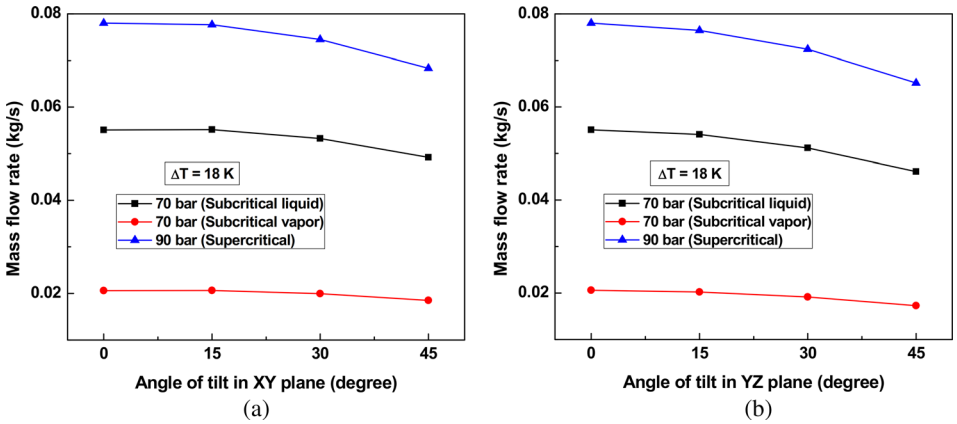

Fig. 5(*a*) Variation in mass flow rate with angle of tilt in *XY* plane and (*b*) variation in mass flow rate with angle of tilt in *YZ* plane

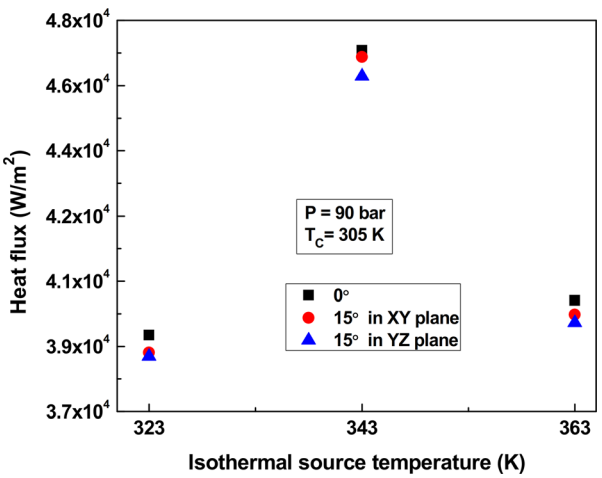

Fig. 6 Variation in heat flux with source temperature

operating condition of the loop. If the operating condition is near the pseudocritical region, then higher heat flux is obtained due to very good thermophysical properties. Results also show that tilting loop in *XY* plane yields slightly higher heat flux than tilting loop in *YZ* plane.

3.5 Effect of Viscous Dissipation and Axial Conduction on Heat Transfer Rate. Table 5 shows the effect of viscous dissipation and wall axial conduction on heat transfer rate. Results show that heat transfer rate is higher in the case of "with axial conduction and viscous dissipation" but the difference is not significant. Compared to axial conduction, viscous dissipation seems to have no or less effect especially at low heat transfer rates. The effect may vary for different operating conditions, wall thicknesses, and wall materials.

3.6 Effect of Tilt on Stability of the Loop. Figures 7(*a*)–7(*f*) show the transient result (temperature and mass flow rate) for different operating conditions and tilt angles. All the results are obtained at the center of the riser of the loop. Results show that tilting in *XY* plane suppresses the fluctuation of flow parameters for all the operating conditions chosen in the study. Startup time as well as time to reach steady-state is also less in the case of tilt in *XY* plane. This can also be seen that the fluctuation in flow parameters in the case of 0 deg and 15 deg (*YZ* plane) is same, which show that there is no significant effect of tilting loop in *YZ* plane. Since there is large fluctuation in thermophysical properties near pseudocritical region (supercritical case), effect of tilt angles can be seen on startup time (Figs. 6(*a*) and 6(*b*)). Startup time in the case of tilt in *YZ* plane is more than the other cases due to increase in relative friction in compared to effective height of the loop. Height of the loop varies from maximum to zero if angle of tilt varies from 0 deg to 90 deg in *YZ* plane or in other words loop becomes horizontal at 90 deg tilt in *YZ* plane and heat transfer rate becomes zero. Conversely, in case of tilt in *XY* plane, heat transfer rate becomes zero at a tilt of 180 deg.

Tilting loop in *YZ* plane does not make any difference in symmetry of the loop. Judging flow direction is difficult in this case (*YZ* plane), whereas tilting in *XY* plane makes a loop thermally and geometrically unsymmetrical. It has been observed that if loop is tilted clockwise then circulation of fluid inside the loop is also clockwise and vice versa in all the cases considered in the present study. So more stable behavior of the loop can be assured with a small angle of tilt of the loop in *XY* plane than in *YZ* plane.

3.7 Validation of Obtained Results With Published Data. In order to validate the results obtained from the CFD simulation, an additional comparison was carried out employing the experimental data reported earlier by Vijayan [19] for a water-based NCL and with numerical results reported earlier by Yadav et al. [13] for a CO_2-based NCL. Comparison is made in terms of nondimensional parameters, namely, Reynolds number (Re) and modified Grashof number (Gr_m) calculated at the average temperature (T_{avg}) of the loop.

Table 5 Effect of viscous dissipation and wall axial conduction on heat transfer rate

Operating conditions	Q (with viscous dissipation and axial conduction) (W)	Q (without axial conduction in wall) (W)	Q (without viscous dissipation and wall axial conduction) (W)
70 bar, $T_C = 274$ K, $T_H = 292$ K	730.5	726	726
70 bar, $T_C = 305$ K, $T_H = 323$ K	297	295	295
90 bar, $T_C = 305$ K, $T_H = 323$ K	2217	2204	2210

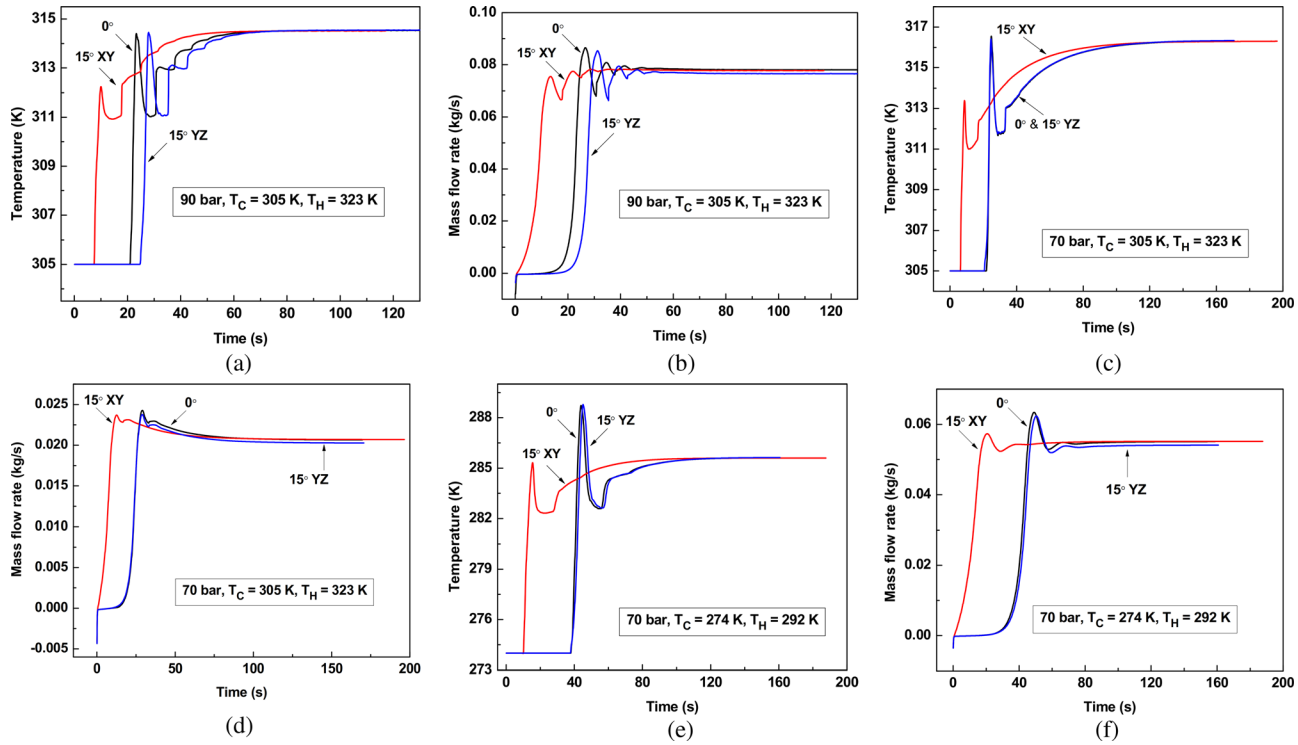

Fig. 7 (*a*) Variation in temperature for different tilt angles (supercritical), (*b*) variation in mass flow rate for different tilt angles (supercritical), (*c*) variation in temperature for different tilt angles (subcritical vapor), (*d*) variation in mass flow rate for different tilt angles (subcritical vapor), (*e*) variation in temperature for different tilt angles (subcritical liquid), and (*f*) variation in mass flow rate for different tilt angles (subcritical liquid)

The Vijayan correlation [19] for turbulent flow (experimental) is expressed as

$$\mathrm{Re} = 1.96(\mathrm{Gr}_m d/L_t)^{\frac{1}{2.75}} \tag{30}$$

The correlation given by Yadav et al. [13] for turbulent flow (numerical) is expressed as

$$\mathrm{Re} = 2.066(\mathrm{Gr}_m d/L_t)^{\frac{1}{2.77}} \tag{31}$$

Effect of tilt angle was not considered in the above correlations. Figure 8 shows that even though the data trends agree reasonably well, significant quantitative difference exists between the present prediction and the previously reported measured data. This may be attributed to the effect of tilting of loop.

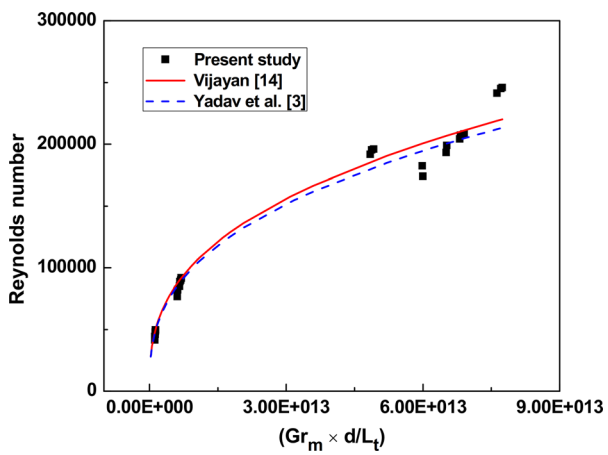

Fig. 8 Validation of obtained result with experimental data

4 Conclusions

Transient simulation of the three-dimensional model of a CO_2-based rectangular NCL has been implemented employing CFD tools. The simulation considers several significant phenomena such as viscous dissipation in fluid, axial conduction in the fluid as well as in the solid wall. Standard RNG k–ε model has been used for turbulent flow. Results are obtained for different angles of tilt for subcritical (liquid and vapor) as well as supercritical CO_2.

The following conclusions could be drawn from this study:

(i) As angle of tilt increases, heat transfer rate and mass transfer rate decrease in both the planes (*XY* and *YZ*).
(ii) Heat transfer rate/heat flux is slightly higher in the case of tilting in *XY* plane.
(iii) Heat transfer rate/heat flux is higher in the case of supercritical phase compared to subcritical phase (liquid and vapor).
(iv) Startup time as well as time to reach steady-state is less in the case of tilt in *XY* plane.
(v) Fluctuation in flow parameters is also less in the case of tilt in *XY* plane.
(vi) A small angle of tilt in *XY* plane provides stable flow (unidirectional) in the present range of study.

Nomenclature

A = area
c_p = specific heat capacity
C_v = constant
C_μ, $C_{1\varepsilon}$, $C_{2\varepsilon}$, $C_{3\varepsilon}$ = parameters in RNG model equations
d = diameter of inner pipe or loop diameter
E = energy
f = friction factor
g = gravitational acceleration
G_b = turbulent kinetic energy due to buoyancy
G_k = turbulent kinetic energy due to mean velocity gradient

Gr = Grashof number
Gr_m = modified Grashof number
h = heat transfer coefficient
H_0 = total height of vertical pipes
k = turbulent kinetic energy
L = length of sink/source
L_c = characteristic length
L_t = total length of the loop
L_0 = total length of a horizontal pipe
L_1 = adiabatic pipe length on horizontal pipe
m = mass flow rate
p P = pressure of fluid
Pr = Prandtl number
Pr_t = turbulent Prandtl number
Q = heat transfer rate
r = radius of loop
R = radius of curvature for bends
R_ε = parameters in RNG model equations
Re = Reynolds number
S = strain tensor
t = time
T = temperature
u, v, V = velocity
x = x-coordinate location

Greek Symbols

α, α_0 = thermal diffusivity
α_k, α_ε = parameters in RNG model equations
β = volumetric expansion coefficient
ΔT = temperature difference across the CHX/HHX
ε = turbulence dissipation rate
η = parameter in RNG model
λ = thermal conductivity
μ = dynamic viscosity
μ_t, μ_{eff} = viscosity parameters in RNG model
ρ = density of fluid
$\bar{\bar{\tau}}$ = stress tensor

Subscripts

avg = average
C = sink
CO_2 = carbon dioxide
eff = effective
f = fluid
H = source
i = x-direction/internal
j = y-direction
m = modified, bulk mean
r = radial direction
ref = reference
s = solid, wall
w = wall
z = axial direction
θ = azimuthal direction

References

[1] Wang, K., Eisele, M., Hwang, Y., and Radermacher, R., 2010, "Review of Secondary Loop Refrigeration Systems," Int. J. Refrig., **33**(2), pp. 212–234.
[2] Kumar, K. K., and Ramgopal, M., 2009, "Carbon Dioxide as Secondary Fluid in Natural Circulation Loops," Proc. Inst. Mech. Eng., Part E, **223**(3), pp. 189–194.
[3] Yadav, A. K., Bhattacharyya, S., and Ramgopal, M., 2014, "On the Suitability of Carbon Dioxide in Forced Circulation Type Secondary Loops," Int. J. Low Carbon Technol., **9**(1), pp. 85–90.
[4] Dostal, V., Hejzlar, P., and Driscoll, M. J., 2006, "The Supercritical Carbon Dioxide Power Cycle: Comparison to Other Advanced Power Cycles," Nucl. Technol, **154**(3), pp. 283–301.
[5] Bondioli, P., Mariani, C., Mossa, E., Fedelli, A., and Muller, A., 1992, "Lampante Olive Oil Refining With Supercritical Carbon Dioxide," J. Am. Oil Chem. Soc., **69**(5), pp. 477–480.
[6] Fourie, F. C. V. N., Schwarz, C. E., and Knoetze, J. H., 2008, "Phase Equilibria of Alcohols in Supercritical Fluids—Part I: The Effect of the Position of the Hydroxyl Group for Linear C8 Alcohols in Supercritical Carbon Dioxide," J. Supercrit. Fluids, **47**(2), pp. 161–167.
[7] Yamaguchi, H., Zhang, X. R., and Fujima, K., 2008, "Basic Study on New Cryogenic Refrigeration Using CO_2 Solid–Gas Two Phase Flow," Int. J. Refrig., **31**(3), pp. 404–410.
[8] Ochsner, K., 2008, "Carbon Dioxide Heat Pipe in Conjunction With a Ground Source Heat Pump (GSHP)," Appl. Therm. Eng., **28**(16), pp. 2077–2082.
[9] Kim, D. E., Kim, M. H., Cha, J. E., and Kim, S. O., 2008, "Numerical Investigation on Thermal–Hydraulic Performance of New Printed Circuit Heat Exchanger Model," Nucl. Eng. Des., **238**(12), pp. 3269–3276.
[10] Kreitlow, D. B., and Reistad, G. M., 1978, "Thermosyphon Models for Downhole Heat Exchanger Application in Shallow Geothermal Systems," ASME J. Heat Transfer, **100**(4), pp. 713–719.
[11] Torrance, K. E., 1979, "Open-Loop Thermosyphons With Geological Application," ASME J. Heat Transfer, **101**(4), pp. 677–683.
[12] NIST Standard Reference Database REFPROP, Version 9.1, 2013.
[13] Yadav, A. K., Ramgopal, M., and Bhattacharyya, S., 2012, "CO_2 Based Natural Circulation Loops: New Correlations for Friction and Heat Transfer," Int. J. Heat Mass Transfer, **55**(17–18), pp. 4621–4630.
[14] Rieberer, R., 2005, "Naturally Circulation Probes and Collectors for Ground-Coupled Heat Pumps," Int. J. Refrig., **28**(8), pp. 1308–1315.
[15] Zhang, X. R., and Yamaguchi, H., 2007, "An Experimental Study on Evacuated Tube Solar Collector Using Supercritical CO_2," Appl. Therm. Eng., **28**(10), pp. 1225–1233.
[16] Zimmermann, A. J. P., and Melo, C., 2014, "Analysis of a R744 Two Phase Loop Thermosyphon Applied to the Cold End of a Stirling Cooler," Appl. Therm. Eng., **73**(1), pp. 549–558.
[17] Rieberer, R., Karl, M., and Hermann, H., 2004, "CO_2 Two-Phase Thermosyphon as a Heat Source System for Heat Pumps," Proceedings of the 6th IIR-Gustav Natural Working Fluids Conference, Glasgow UK.
[18] Welander, P., 1967, "On the Oscillatory Instability of a Differential Heated Fluid Loop," J. Fluid Mech., **29**(1), pp. 17–30.
[19] Vijayan, P. K., 2002, "Experimental Observations on the General Trends of the Steady State and Stability Behaviour of Single-Phase Natural Circulation Loops," Nucl. Eng. Des., **215**(1–2), pp. 139–152.
[20] Cammarata, L., Fichera, A., and Pagano, A., 2003, "Stability Maps for Rectangular Circulation Loops," Appl. Therm. Eng., **23**(8), pp. 965–977.
[21] Mousavian, S. K., Misale, M., D'Auria, F., and Salehi, M. A., 2004, "Transient and Stability Analysis in Single Phase Natural Circulation," Ann. Nucl. Energy, **31**(10), pp. 1177–1198.
[22] Jain, P. K., and Rizwan-uddin, 2008, "Numerical Analysis of Supercritical Flow Instabilities in a Natural Circulation Loop," Nucl. Eng. Des., **238**(8), pp. 1947–1957.
[23] Chen, L., Zhang, X. R., Yamaguchi, H., and Liu, Z.-S., 2010, "Effect of Heat Transfer on the Instabilities and Transitions of Supercritical CO_2 Flow in a Natural Circulation Loop," Int. J. Heat Mass Transfer, **53**(19–20), pp. 4101–4111.
[24] Misale, M., Garibaldi, P., Passos, J. C., and Bitencourt, G. D., 2007, "Experiments in a Single Phase Natural Circulation Mini-Loop," Exp. Therm. Fluid Sci., **31**(8), pp. 1111–1120.
[25] Yadav, A. K., Ramgopal, M., and Bhattacharyya, S., 2014, "Transient Analysis of Subcritical/Supercritical Carbon Dioxide Based Natural Circulation Loops With End Heat Exchangers: Numerical Studies," Int. J. Heat Mass Transfer, **79**, pp. 24–33.
[26] Yang, J., Oka, Y., Ishiwatari, Y., Liu, J., and Yoo, J., 2007, "Numerical Investigation of Heat Transfer in Upward Flow of Supercritical Water in Circular Tubes and Tight Fuel Rod Bundles," Nucl. Eng. Des., **237**(4), pp. 420–430.
[27] Lisboa, P. F., Fernandes, J., Simoes, P. C., Mota, J. P. B., and Saatdjian, E., 2010, "Computational-Fluid-Dynamics Study of a Kenics Static Mixer as a Heat Exchanger for Supercritical Carbon Dioxide," J. Supercrit. Fluids, **55**(1), pp. 107–115.
[28] Chen, L., and Zhang, X. R., 2011, "Simulation of Heat Transfer and System Behavior in a Supercritical CO_2 Based Thermosyphon: Effect of Pipe Diameter," ASME J. Heat Transfer, **133**(12), p. 122505.
[29] Vijayan, P. K., and Austregesilo, H., 1994, "Scaling Laws for Single-Phase Natural Circulation Loops," Nucl. Eng. Des., **152**(1–3), pp. 331–347.
[30] Zhang, X. R., Chen, L., and Yamaguchi, H., 2010, "Natural Convective Flow and Heat Transfer of Supercritical CO_2 in a Rectangular Circulation Loop," Int. J. Heat Mass Transfer, **53**(19–20), pp. 4112–4122.
[31] Yadav, A. K., Ramgopal, M., and Bhattacharyya, S., 2012, "CFD Analysis of a CO_2 Based Natural Circulation Loop With End Heat Exchangers," Appl. Therm. Eng., **36**, pp. 288–295.
[32] Launder, B. E., and Spalding, D. B., 1974, "The Numerical Computation of Turbulent Flows," Comput. Methods Appl. Mech. Eng., **3**(2), pp. 269–289.
[33] Kumar, K. K., and Ramgopal, M., 2009, "Steady-State Analysis of CO_2 Based Natural Circulation Loops With End Heat Exchangers," Appl. Therm. Eng., **29**(10), pp. 1893–1903.